J Mater Sci (2008) 43:6324–6330
DOI 10.1007/s10853-008-2895-4

Hot deformation of AA6082-T4 aluminum alloy

Ehab A. El-Danaf · Abdulhakim A. AlMajid · Mahmoud S. Soliman

Received: 3 October 2007 / Accepted: 22 July 2008 / Published online: 16 August 2008

Abstract High-temperature tensile deformation of 6082-T4 Al alloy was conducted in the range of 623–773 K at various strain rates in the range of 5×10^{-5} to 2×10^{-2} s^{-1}. Stress dependence of the strain rate revealed a stress exponent, n of 7 throughout the ranges of temperatures and strain rates tested. This stress exponent is higher than what is usually observed in Al–Mg alloys under similar experimental conditions, which implies the presence of threshold stress. This behavior results from dislocation interaction with second phase particles (Mg_2Si). The experimental threshold stress values were calculated, based on the finding that creep rate is viscous glide controlled, based on creep tests conducted on binary Al–1Mg at 673 K, that gave n a value of 3. The threshold stress (σ_o) values were seen to decrease exponentially with temperature. The apparent activation energy for 6082-T4 was calculated to be about 245 kJ mol^{-1}, which is higher than the activation energy for self-diffusion in Al ($Q_d = 143$ kJ mol^{-1}) and for the diffusion of Mg in Al (115–130 kJ mol^{-1}). By incorporating the threshold stress in the analysis, the true activation energy was calculated to be about 107 kJ mol^{-1}. Analysis of strain rate dependence in terms of the effective stress ($\sigma - \sigma_o$) using normalized parameters, revealed a single type of deformation behavior. A plot of normalized strain rate ($\dot{\varepsilon}kT/DGb$) versus normalized effective stress ($\sigma - \sigma_o$)/G, on a double logarithmic scale, gave an n value of 3.

Introduction

The hot workability of aluminum and its alloys has been of both technical and scientific interest in the last decade [1–11]. The 6xxx-group contains magnesium and silicon as major alloying elements. These multiphase alloys belong to the group of commercial aluminum alloys, in which relative volume; chemical composition and morphology of structural constituents exert significant influence on their useful properties [12–14]. Al–Mg–Si alloys have recently been used for automotive body sheet panel for weight saving. However, this is partially limited by poor press formability in these alloys, though both specific stiffness and strength are sufficiently high. Several studies [6–14] demonstrated the fact that high-temperature deformation of aluminum alloys is controlled by dynamic recovery; the flow curves in general exhibit strain hardening to a steady state, even though in some conditions a moderate peak is observed. The formation of solute atom atmosphere hinder dislocation glide raising the flow stress, but precipitation of fine particles is a more effective source of strengthening. 6xxx aluminum alloys are known to be heat treatable to form precipitates, but since precipitation hardening assume various forms (under-aged, peak-aged, and over-aged), thus not in all conditions it would be beneficial to the high-temperature characteristics of the alloy, as for over aging due to the large particle size and spacing precipitates have a minor strengthening effect and the solute level is low [15, 16].

Ehab A. El-Danaf—on leave from the Department of Mechanical Design and Production, College of Engineering, Cairo University, Egypt.

E. A. El-Danaf (✉) · A. A. AlMajid · M. S. Soliman
Mechanical Engineering Department, College of Engineering, King Saud University, P.O. Box 800, Riyadh, Saudi Arabia
e-mail: edanaf@ksu.edu.sa

A. A. AlMajid
e-mail: aalmajid@ksu.edu.sa

M. S. Soliman
e-mail: solimanm@ksu.edu.sa

Creep (strain rate $\dot{\varepsilon} < 10^{-4}$ s^{-1}) and hot working ($\dot{\varepsilon} = 10^{-2}$to 10^{+2} s^{-1}) of pure metals and metallic solid-solution alloys, occur at high temperature ($T > 0.5\ T_m$, where T_m is the absolute melting point), are equivalent during the steady state. The stress dependence of $\dot{\varepsilon}$ is usually described by a power function; in the so-called power law regime, such as Eq. 1 [17]:

$$\dot{\varepsilon} = A\sigma^n \exp\left(\frac{-Q_a}{RT}\right) \quad (1)$$

where σ is the stress, n is the stress exponent, Q_a is the apparent activation energy, R is the universal gas constant, T is the absolute temperature, and A is a constant. The value of n and other characteristics were used to classify metals and alloys [17, 18]. For Al–Mg alloys [19–23] and Al–Cu alloys [24–26] which exhibit large solid solution hardening (high atomic-misfit parameter), the measured values of n are close to 3, and are characterized by solute drag mechanism resulting from elastic interaction between dislocations and solute atoms due to the size effect. This type of behavior has been termed as class I or alloy class [17, 18]. On the other hand, for pure metals and some solid solution alloys, usually with low atomic-misfit parameter, the values of n are close to 5 and the strain rate is a function of stacking fault energy. This behavior is termed as class II or pure metal class [17, 18]. It is believed that some form of dislocation climb is the rate controlling process. It was suggested that dislocation climb and viscous glide are two sequential processes in solid solution alloys and that the slower process controls the deformation mechanism under the imposed experimental conditions [27]. It was also suggested that other viscous drag processes can operate sequentially with the solute drag mechanism, but the contribution of these processes to the total drag force depend on the alloy system [28].

Comparing the hot formability of aluminum binary solid-solution alloys with that of aluminum alloys produced by ingot metallurgy (IM), powder metallurgy (PM), and of aluminum-based metal–matrix composites [29, 30] suggests that the latter materials are characterized by the presence of the threshold stress σ_o, resulting from the interaction of the fine dispersed particles in these alloys with the moving lattice dislocations. Under this condition, the deformation process is not driven by the applied stress but rather by an effective stress σ_e ($=\sigma - \sigma_o$). Hypereutectic Al–17Si was investigated by Spigarelli et al. [31], and found a stress exponent close to 4–5. Although the magnitude of the stress exponent observed was equivalent to that observed in pure Al, the apparent activation energy for creep was higher (Q = 210 kJ mol^{-1}) than the activation energy for self-diffusion in Al (Q_d = 143 kJ mol^{-1}) [17]. This observation indicated that creep response should be addressed by taking into account more articulated models than the one given by the constitutive Eq. 1 shown above. They rationalized both the magnitude of the stress exponent and the apparent activation energy for creep, based on threshold-stress concept which arises due to interaction between fine particles and dislocation [9, 29–31]. They calculated the true activation energy, taking into account the threshold stress value, to be 160 kJ mol^{-1}, which is comparable for that of pure Al.

The objective of the present study is to examine in detail the high-temperature deformation of a 6082 Al alloy naturally aged (T4 condition) over a wide range of stresses, strain rates, and temperatures to examine the presence of the threshold stress and find out the rate controlling mechanisms in the deformation of the alloy. This alloy is characterized by the presence of second phase particles Mg_2Si. The silicon will be in solid solution only above 530 °C [13].

Experimental procedure

High-temperature tensile tests were carried out on as received 6082 aluminum alloy (T4 condition), whose composition in wt.% is as follows: 0.99 Mg, 1.46 Si, 0.58 Mn, 0.36 Fe, and rest is Al. The alloy was supplied as rods with an average grain size of about 58 μm as calculated by the line intercept method. The room-temperature mechanical properties are yield strength of 250 MPa, ultimate strength of 300 MPa, and ductility of 10%. Flat tensile specimens of 12 mm gage length and 5 × 3 mm^2 cross-sectional area were machined such that the tensile axis was parallel to the drawing direction. The tension tests were carried out using an Instron machine, model 1197 with a resistance furnace containing three heating zones. All specimens were tested in air and soaked in the furnace at the testing temperature for 30 min before testing to establish thermal equilibrium. Four temperatures were used in the range 623–773 K with an interval of 50 K; these temperatures were selected as they simulate the real industrial forming conditions of this alloy. The temperature was controlled using a thermocouple connected to the middle of the gauge section. At each temperature different constant speeds were used to impose initial strain rates in the range of 5×10^{-5} s^{-1} to 2×10^{-2} s^{-1}. The strain rates quoted thereafter represent the initial strain rates calculated from the initial gage length of the specimens. True stress–strain curves were plotted and the steady-state stress, and in some conditions peak flow stress, when steady state do not prevail specially at high strain rates, were depicted. In addition, a few creep experiments were conducted on Al–1 wt.% Mg, which has almost similar Mg content as the 6082 Al alloy tested here, at 673 K in the solid solution range at similar strain rates to investigate the creep rate controlling mechanism.

Results

True stress–strain curves

Figure 1a–d shows the true stress–true strain curves at 623, 673, 723, and 773 K for different initial strain rates. The results show the high strain rate sensitivity exhibited by the alloy at these temperatures. The true stress–strain response can be divided into three regions. In region I, strain hardening region where the stress increases with strain until it reaches almost constant value in region II that represents the steady-state stress at the applied strain rate. In region III, necking and/or cracking occurs leading to a decrease in the flow stress and thereafter fracture.

Stress dependence of strain rate

The stress dependence of the strain rate under steady-state condition at constant temperature is determined by plotting the strain rate, $\dot{\varepsilon}$ as a function of the steady-state stress, σ on a double logarithmic scale. Figure 2 shows this form of plot for four different temperatures 623, 673, 723, and 773 K. Examination of the data of this figure reveals that for the range of strain rates and temperatures tested the data points fall on line segments with stress exponent of 7 and that power law break down is not evident as the curves are linear to high strain rates.

Ductility

Figure 3 shows the results of ductility measurements in which the elongation at fracture e_f % (=$\Delta L_f/L_o$, where ΔL_f is the increase in length at fracture and L_o is the initial length of the specimen), is plotted as a function of initial strain rate $\dot{\varepsilon}$ at various testing temperatures. As seen in the figure, the ductility curves for temperatures of 773, 723, and 673 K display a maxima profile with a peak in the strain-rate range of 6×10^{-4} to 3×10^{-3} s^{-1}; the peak value of ductility increases with increasing temperature. The e_f % values exhibit a marked increase at 773 K compared to the other temperatures; a maximum of 93% is obtained at this temperature compared to a maximum value of 30% at 673 K. On the other hand, at 623 K the ductility continuously decreases with strain rate. This behavior is similar to that previously reported for aluminum alloys [4, 5].

Apparent activation energy

Using Eq. 1, the apparent activation energy Q_a can be calculated at constant strain rate as

$$Q_a = nR\left[\frac{\partial \ln \sigma}{\partial(1/T)}\right]_{\dot{\varepsilon}} \quad (2)$$

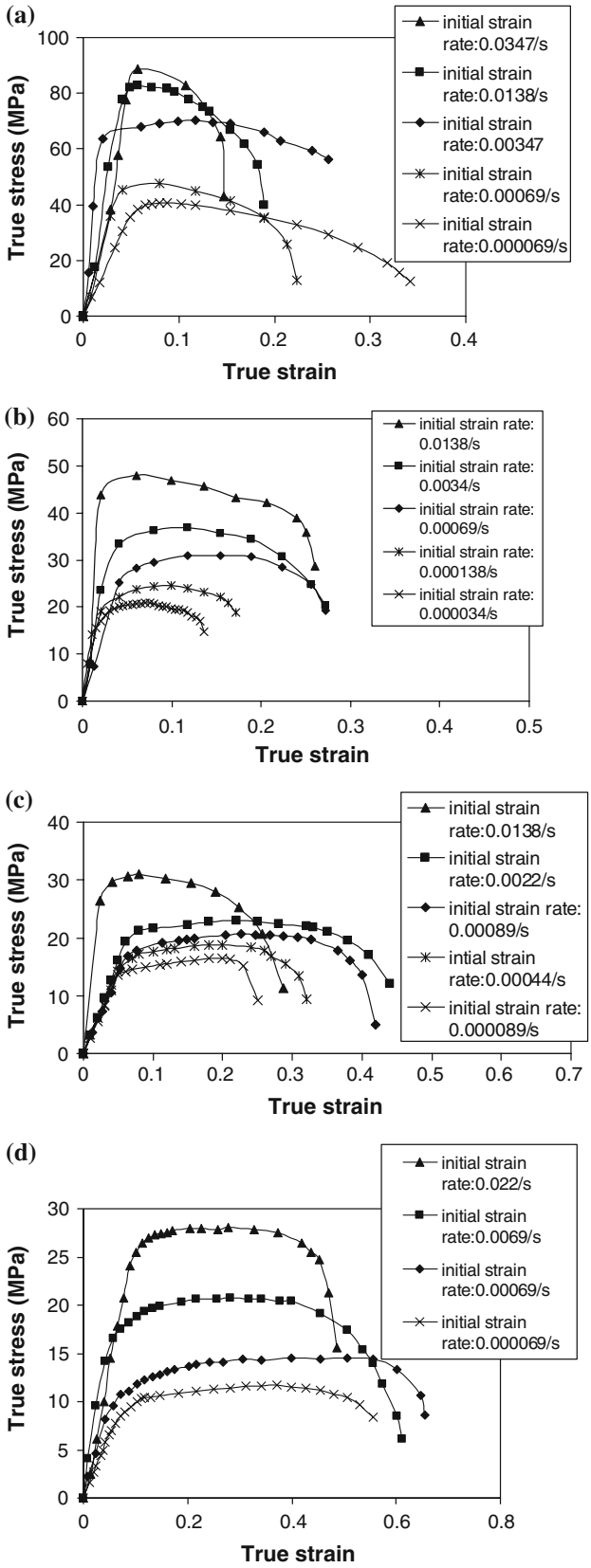

Fig. 1 True stress–strain curves at; (**a**) 623 K, (**b**) 673 K, (**c**) 723 K, and (**d**) 773 K at various initial strain rates

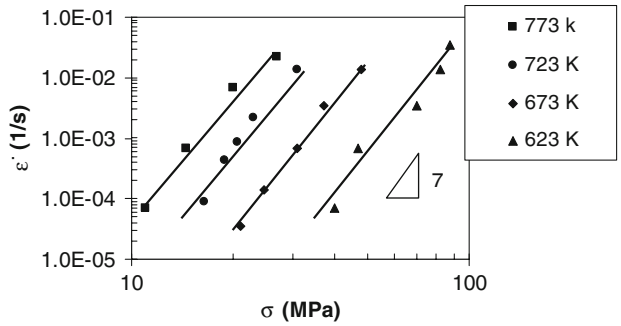

Fig. 2 Stress dependence of the strain rate at different temperatures, showing the value of stress exponent

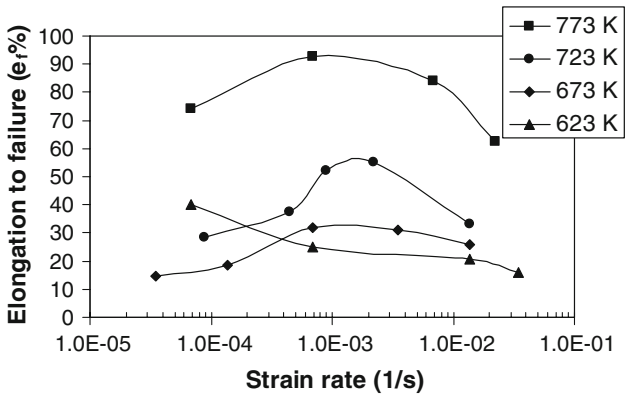

Fig. 3 Elongation at failure, e_f % as a function of temperature and strain rate

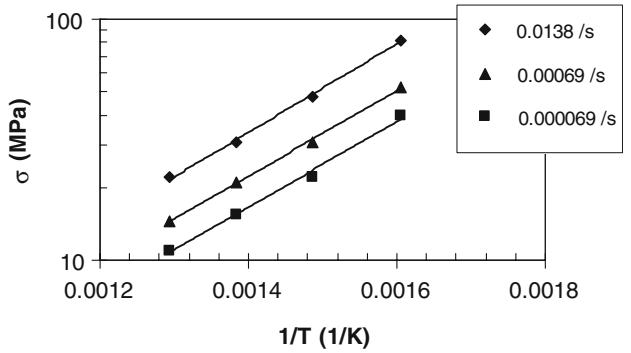

Fig. 4 A plot of log stress versus the reciprocal of absolute temperature at various strain rates

Figure 4 shows a plot of log σ versus $(1/T)$ at three different strain rates. The data points at constant strain rate fall on a segment of straight line whose slope is equal to $(Q_a/2.3nR)$, which gives Q_a a value of 245 kJ mol^{-1}. In calculating Q_a, the value of n was taken as 7 as inferred from Fig. 2.

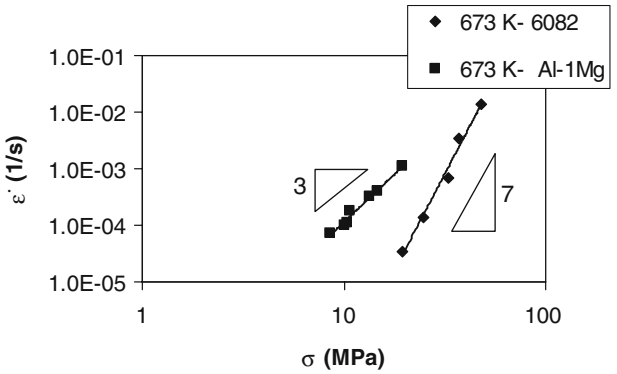

Fig. 5 Stress dependence of the strain rate at 673 K, for binary Al–1Mg and 6082 Al alloy

Discussion

Threshold stress

The threshold-stress behavior is characterized by two points [29, 30]: (i) a high value of stress exponent, n that continuously increases with decreasing stress and (ii) a high value of activation energy above that reported for self-diffusion. While the second point is clearly obvious in the results of the present investigation, point one is not. Figure 2 shows that the value of n is independent of stress and temperature and has a constant value of ≈ 7. This lack of agreement with point one may be attributed to the limited range of strain rate applied in the present investigation. This behavior is similar to that recently reported for Al–17 Si alloy [31]; constant n value ~ 5 and high activation energy ($Q = 210$ kJ mol^{-1}). This high value of n for the present alloy is higher than what is usually reported for binary Al–Mg alloys ($n = 3$) at similar temperatures and strain rates [19–23]. In addition, the creep data at 673 K for a binary Al–1 Mg investigated in the present study ($n \sim 3$) is compared to the results of 6082 Al alloy at the same temperature, as shown in Fig. 5. The reason for this difference in values of n may arise from the presence of threshold stress, due to the interaction of dislocation with second phase particles (Mg_2Si) present in 6082 Al alloy. This possibility is explored by plotting $\dot{\varepsilon}^{1/3}$ versus σ using a double linear scale as shown in Fig. 6. The data points for each temperature fall on a segment of straight line and the extrapolation of these lines to zero strain rate gives the value of σ_o at each temperature. The values of σ_o are 8.8, 13, 17.9, and 33 MPa at 773, 723, 673, and 623 K, respectively. The present results along with previous studies [7–9, 29] suggest that σ_o is a function of temperature and it decreases with increasing temperature. The temperature dependence of the normalized threshold stress (σ_o/G) is shown in Fig. 7 where log (σ_o/G) is plotted versus $(1/T)$. The value of the shear modulus, G for the alloy as a

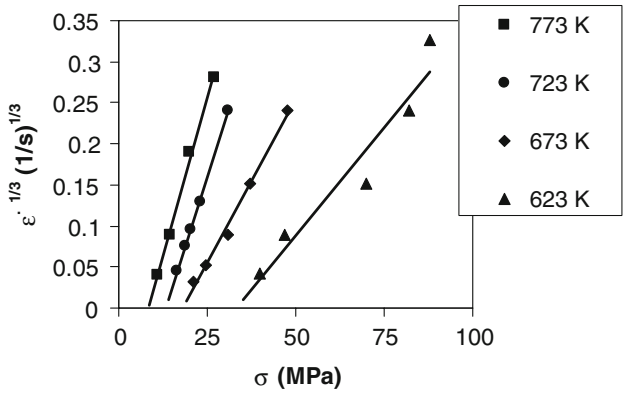

Fig. 6 Double linear plot for $\dot{\varepsilon}^{(1/3)}$ versus stress at different temperatures

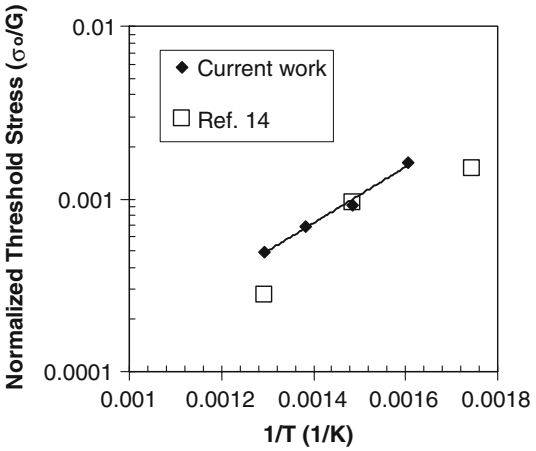

Fig. 7 Semi-logarithmic plot for normalized threshold stress (σ_o/G) versus the reciprocal of absolute temperature from the current work as well as from a previous work [14]

function of temperature is taken as that for pure Al, $G = 3.022 \times 10^4 - 16\ T$ (MPa) [17]. This dependence can be expressed as

$$\left(\frac{\sigma_o}{G}\right) = B_o \exp\left(\frac{Q_o}{RT}\right) \tag{3}$$

where B_o and Q_o are constants having the values of 4×10^{-6} and 31 kJ mol^{-1}, respectively. This behavior is similar to that observed in a number of PM Al alloys and Al metal–matrix composites [29, 30]. The results of a previous work [14] is also presented in Fig. 7. While the results showed agreement at 673 K, there was a large discrepancy at lower and higher temperatures. This inconsistency in both results may be due to the different heat treatment adopted in [14] (over aging the samples at the respective testing temperature for 24 h), different mode of testing (torsion) and the different procedure used for calculating the threshold stress values. When the strain rates are plotted as a function of the effective stress $(\sigma - \sigma_o)$, the stress exponent n inferred is close to 3 as shown in Fig. 8.

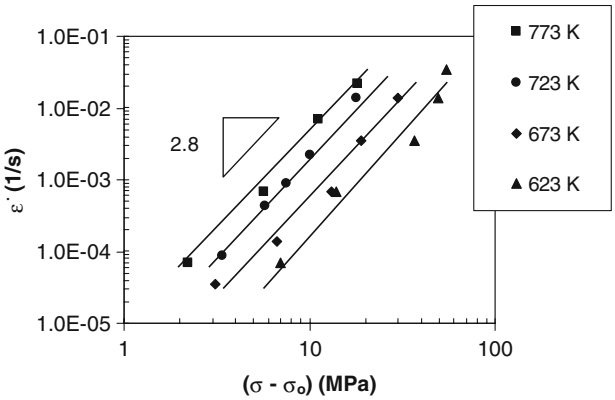

Fig. 8 A double logarithmic plot for effective stress dependence on strain rate

True activation energy

Under the presence of threshold stress, Eq. 1 can be modified such that the applied stress is replaced by an effective stress, $(\sigma - \sigma_o)$. This equation when written in the normalized form is given by:

$$\frac{\dot{\varepsilon}kT}{DGb} = A_o\left(\frac{\sigma - \sigma_o}{G}\right)^n \tag{4a}$$

with

$$D = D_o \exp\left(\frac{-Q}{RT}\right) \tag{4b}$$

where k is Boltzmann's constant, b is the magnitude of Burgers vector, A_o is a dimensionless constant, Q is the true activation energy for the diffusion process that controls the deformation mechanism, and D_o is a frequency factor. Equation 4, at constant strain rate, can be rearranged in the form

$$\exp\left(\frac{Q}{RT}\right) = C\left(\frac{G}{T}\right)\left(\frac{\sigma - \sigma_o}{G}\right)^n \tag{5}$$

where C is a constant. Taking the natural logarithm of Eq. 4 and differentiating with respect to $(1/T)$, the value of Q can be written as

$$Q = R\frac{\partial \ln\left[\frac{G}{T}\left(\frac{\sigma-\sigma_o}{G}\right)^n\right]}{\partial\left(\frac{1}{T}\right)} \tag{6}$$

Equation 6 is used to calculate the true activation energy by plotting $\log\left[\frac{G}{T}\left(\frac{\sigma-\sigma_o}{G}\right)^3\right]$ versus $(1/T)$ as shown in Fig. 9. The value of Q was determined at three various strain rates in the temperature range of 623–773 K. As shown in the figure, the data points fall on segments of parallel straight lines giving Q a constant value independent of strain rate. The average value of Q was calculated as 107 kJ mol^{-1}. This value is very close to that reported for diffusion of Mg in Al (115–130 kJ mol^{-1}) [32, 33]. A value of $Q = 100$ kJ mol^{-1}

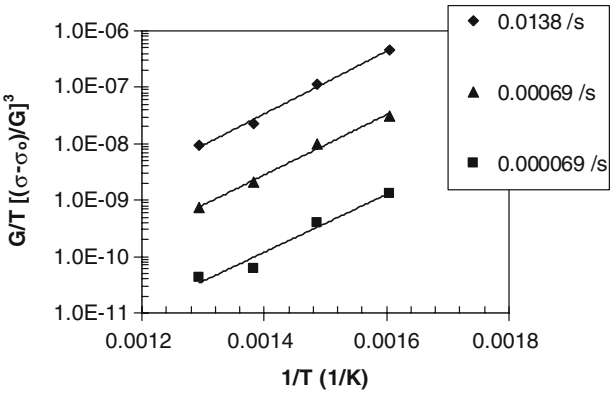

Fig. 9 Semi-logarithmic plot of $(G/T)[(\sigma - \sigma_o)/G]^3$ versus $(1/T)$ for calculating the true activation energy

was reported for creep in Al–3wt.% Mg at a temperature of 673 K when n is equal to 3 [34].

Normalized strain rates

Because of the similarity between the value of Q and that for the diffusivity of Mg in Al, the diffusion coefficient of Mg in Al, $D_{Mg} = D_o \exp\left(\frac{-107\times10^3}{RT}\right)$ m^2 s^{-1}, where $D_o = 0.0632 \times 10^{-4}$ m^2 s^{-1} [31], was used in normalizing the data of the 6082 Al alloy. Figure 10 gives the normalized creep rate $(\dot{\varepsilon}kT/DGb)$ versus the normalized effective stress $((\sigma - \sigma_o)/G)$. As shown in the figure, the data points coalesce on one segment of straight line with a slope of 3. For the purpose of comparison, the data of the binary Al–1 Mg alloy are also included in Fig. 10. In normalizing the data for Al–1 Mg, the shear modulus and self-diffusivity of Al were used [17]. A constitutive equation of the deformation behavior of the alloy at present experimental conditions can be written as:

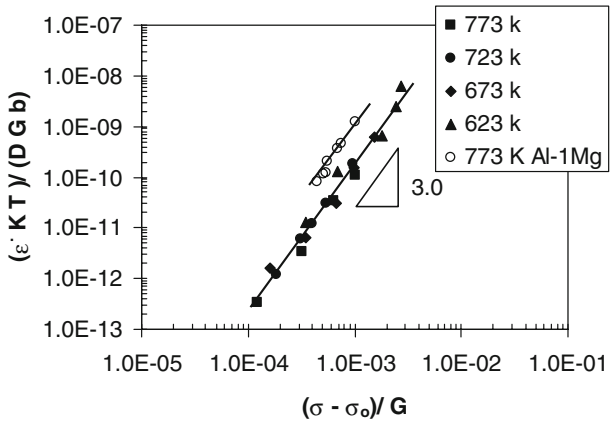

Fig. 10 Normalized strain rate versus normalized effective stress for 6082 alloy and Al–1Mg binary alloy ($\sigma_o = 0$)

$$\left(\frac{\dot{\varepsilon}kT}{DGb}\right) = 0.2\left(\frac{\sigma - \sigma_o}{G}\right)^3 \quad (7)$$

This equation can be used in modeling the forming process of this alloy under similar hot working conditions.

Conclusions

1. The deformation behavior of the AA6082-T4 Al alloy was examined at temperatures ranging from 623 to 773 K in the strain rate range from 10^{-5} to 10^{-2} s^{-1}. The value of n and Q_a were $\sim$7 and 245 kJ mol^{-1}, respectively.
2. Analysis of experimental data of the alloy revealed the presence of a threshold stress that decreases with temperature with an energy term, Q_o, 31 kJ mol^{-1}.
3. By incorporating the threshold stress into the analysis, a plot of the normalized strain rate, $\dot{\varepsilon}kT/DGb$ versus normalized effective stress yielded a stress exponent, n of 3.
4. The calculated true activation energy was close to that for diffusion of Mg in Al and the n value being 3 suggested that viscous glide of dislocations is the rate controlling mechanism.
5. Enhanced ductility was observed in the middle of the strain rate range at high temperatures and decreased with decreasing/increasing strain rate.

Acknowledgements This work was supported by the Research Center at King Saud University, College of Engineering, and SABIC grants (grant # 428/38). This support is highly acknowledged.

References

1. McQueen HJ, Jones JJ (1975) In: Arsenault RJ (ed) Plastic deformation of materials. Academic Press, New York
2. Nakashima H, Iwasaki K, Goto S, Yoshinaga H (1990) Mater Trans JIM 31:35
3. Avramovic-Cingara G, Perovic DD, McQueen HJ (1996) Metall Mater Trans A 27A:3478. doi:10.1007/BF02595440
4. Taleff EM, Lesuer DR, Wadsworth J (1996) Metll Mater Trans A 27A:343. doi:10.1007/BF02648411
5. Taleff EM, Nevland PJ, Krajewski PE (2001) Metall Mater Trans A 32A:1119. doi:10.1007/s11661-001-0123-9
6. Zhang H, McQueen HJ (2001) Mater Sci Eng A 319–321:711. doi:10.1016/S0921-5093(01)01041-3
7. Kaibyshev R, Sitdikov O, Mazurina I, Lesuer DR (2002) Mater Sci Eng A 334:104. doi:10.1016/S0921-5093(01)01777-4
8. Marquis EA, Seidman DN, Dunand DC (2003) Acta Mater 51:4751. doi:10.1016/S1359-6454(03)00288-X
9. Kaibyshev R, Musin F, Avtokratova E, Motohashi Y (2005) Mater Sci Eng A 392:373. doi:10.1016/j.msea.2004.10.002
10. McQueen HJ (2002) Metall Mater Trans A 33A:345. doi:10.1007/s11661-002-0096-3
11. McQueen HJ, Kassner ME (2005) Mater Sci Eng A 410–411:58. doi:10.1016/j.msea.2005.08.048
12. Kovacs-Csetenyi E, Chinh NQ, Kovacs I (1996) Mater Sci Forum 217–222:1175

13. Ronning B, Nord-Varhaung K, Furu T, Nes E (2000) Mater Sci Forum 331–337:571
14. Spigarelli S, Evangelista E, McQueen HJ (2003) Scr Mater 49:179. doi:10.1016/S1359-6462(03)00206-9
15. Mrowka-Nowotnik G, Sieniawski J (2005) J Mater Processing Technology 162–163:367. doi:10.1016/j.jmatprotec.2005.02.115
16. Gracio JJ, Barlat F, Rauch EF, Jones PT, Neto VF, Lopes AB (2004) Int J Plast 20:427. doi:10.1016/S0749-6419(03)00095-0
17. Kassner ME, Perez-Prado MT (2000) Prog Mater Sci 45:1. doi:10.1016/S0079-6425(99)00006-7
18. Mohamed FA, Langdon TG (1974) Acta Metall 22:779. doi:10.1016/0001-6160(74)90088-1
19. Yavari P, Mohamed FA, Langdon TG (1981) Acta Metall 29:1495. doi:10.1016/0001-6160(81)90184-X
20. Soliman MS, Mohamed FA (1982) Mater Sci Eng A 55:111. doi:10.1016/0025-5416(82)90090-8
21. Oikawa H, Honda K, Ito S (1984) Mater Sci Eng A 64:237. doi:10.1016/0025-5416(84)90107-1
22. Oikawa H, Sato H, Maruyama K (1985) Mater Sci Eng A 75:21. doi:10.1016/0025-5416(85)90174-0
23. Sato H, Oikawa H (1988) Scr Metall 22:87. doi:10.1016/S0036-9748(88)80311-9
24. Chaudhury B, Mohamed FA (1988) Mater Sci Eng A 101:13. doi:10.1016/0025-5416(88)90787-2
25. Chaudhury B, Mohamed FA (1987) Metall Trans A 18:2105. doi:10.1007/BF02647082
26. Soliman MS (1995) Mater Sci Eng A 201:111. doi:10.1016/0921-5093(95)09776-7
27. Mohamed FA (1983) Mater Sci Eng A 61:149. doi:10.1016/0025-5416(83)90197-0
28. Soliman MS, Mohamed FA (1984) Metall Trans A 15A:1893
29. Mohamed FA (1998) Mater Sci Eng A 245:242. doi:10.1016/S0921-5093(97)00725-9
30. Evangelista E, Spigarelli S (2002) Metall Mater Trans A 33A:373. doi:10.1007/s11661-002-0098-1
31. Spigarelli S, Evangelista E, Gucchieri S (2004) Mater Sci Eng A 387–389:702
32. Hirano K, Fujikawa S (1978) J Nucl Mater 69–70:564. doi:10.1016/0022-3115(78)90275-1
33. Rothman SJ, Peterson NL, Nowicki LJ, Robinson LC (1974) Phys Status Solidi B 63:K29–K33. doi:10.1002/pssb.2220630151
34. Hamersky M, Lukac P, Trojanova Z, Pink E (1991) Mater Sci Eng A 148:7. doi:10.1016/0921-5093(91)90860-P